January 2001

Consistent Phase Estimation for Recovering Depth From Moiré Interferograms

Thomas Bülow
University of Pennsylvania

University of Pennsylvania Department of Computer and Information Science Technical Report No. MS-CIS-01-14.

Consistent Phase Estimation for Recovering Depth From Moiré Interferograms

Abstract

Moiré interferometry is a common tool if depth estimation from a single image frame is desired. It uses the interference of periodic patterns to measure the topology of a given surface. The actual depth estimation relies on the consistent phase estimation from the interferogram. We show that this task can be simplified by estimating the image phase and the local image orientation simultaneously, followed by a processing step called orientation unwrapping which is introduced in this paper. We compare two methods for extracting image phase and orientation and present experimental results.

Comments

University of Pennsylvania Department of Computer and Information Science Technical Report No. MS-CIS-01-14.

Consistent Phase Estimation for Recovering Depth from Moiré Interferograms

Thomas Bülow
University of Pennsylvania
GRASP Laboratory

thomasbl@grasp.cis.upenn.edu

MS-CIS-01-14

Abstract

Moiré interferometry is a common tool if depth estimation from a single image frame is desired. It uses the interference of periodic patterns to measure the topology of a given surface. The actual depth estimation relies on the consistent phase estimation from the interferogram. We show that this task can be simplified by estimating the image phase and the local image orientation simultaneously, followed by a processing step called orientation unwrapping which is introduced in this paper. We compare two methods for extracting image phase and orientation and present experimental results.

1. Introduction

Moiré interferometry is a measurement technique which allows the measurement of the topology of a given surface. In this technique a periodic grid is projected onto the surface while an image of the surface is taken through another grid. The Moiré pattern results from the the interference of the two periodic grids.

This technique is used e.g. for measuring model deformations in wind tunnels [16]. A detailed description of the experimental setup in this context can be found e.g. in [1]. Fig. 1 shows two interferograms from this application. Fig. 1(a) shows a model wing of a transport aircraft. The instantaneous deformations and movements of the wing due to aerodynamic load were to be measured. Fig. 1(b) shows the interferogram of a tilt plane plate used as calibration target in the same experiment. The images were taken in the cryogenic European Transonic Wind Tunnel (ETW) in Köln, Germany. The intensity

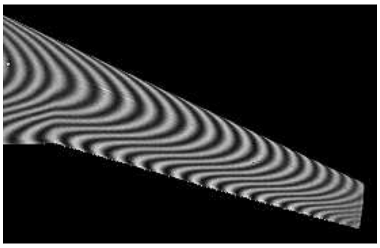

(a)

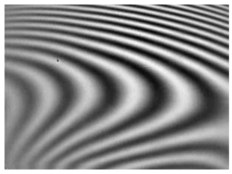

(b)

Figure 1: Two interferograms. **(a)** A model wing. **(b)** A calibration plate.

pattern of the interferograms can be modeled by the function

$$I(m,n) = \frac{I_0}{2}(1 + \cos(\phi(m,n)). \tag{1}$$

I_0 denotes the amplitude of the oscillation. The discrete image coordinates are denoted by (m,n). The support of the image is a rectangular subset D of $\mathbb{Z}^2$, such that we have $(m,n) \in D$. The depth at each point (m,n) in the image is given by

$$z(m,n) = \phi(m,n)\frac{\Delta z}{2\pi} + z_0. \tag{2}$$

Here Δz is the so-called layer distance. This is the distance by which the surface has to be moved in z-direction in order to achieve a phase shift of the the interferogram by 2π. z_0 is an overall offset, which cannot be measured from the interferogram. The above two formulas were taken from [1].

The image processing task which is the subject of this article is the extraction of the local image phase $\phi(m,n)$ from $I(m,n)$ given in (1). We observe two restrictions:

1. Since the cosine-function is 2π-periodic, the phase ϕ can (without further assumptions on the smoothness of the surface) only be evaluated up to 2π.

2. Since the cosine-function is even, we can evaluate ϕ merely up to a sign.

The first restriction is not a severe one, since the smoothness of the surfaces under consideration allows for a simple unwrapping once ϕ is evaluated up to 2π. (Basically phase wrap-arounds can be assumed wherever the difference between two neighboring phase-values is greater than π.) The second restriction is more serious, since the sign of ϕ can flip from pixel to pixel. The automatic corrections of these flips is much more difficult. There is no simple rule for their detection as in the unwrapping task.

We will propose a method for the removal of phase-flips which is based on taking into account information on the local orientation of the Moiré-pattern and a technique which we call orientation unwrapping. Once all phase-flips have been removed there remain two possible global solutions ($(\phi(m,n))_{(m,n)\in D}$ and $(-\phi(m,n))_{(m,n)\in D}$) the correct one of which has to be identified by hand. This is usually done without problem. A preliminary version of this work can be found in [3].

In the following section we will briefly recap phase estimation of 1D signal, as well as the definition of phase in 2D. On the basis of this definition we will describe our approach to the solution of the "phase-flip" problem.

In Sect. 3 we present two methods for the estimation of 2D-phase, which are compared in Sect. 4 by applying them to the real data shown in Fig. 1 as well as to synthetically generated data with known ground-truth. The article is closed by an outlook to further work to be done.

2. Local Phase of Images

2.1. Local Phase in 1D

Given a 1D signal

$$f(x) = a(x)\cos(2\pi u(x)x), \quad u(x), a(x) > 0\, \forall x \in \mathbb{R} \tag{3}$$

we want to extract its *local phase*[1] $\phi(x)$. A way to do this is the construction of the complex or analytic signal which was introduced by Gabor [6]. The analytic signal is defined as the sum of the original signal plus i times its Hilbert transform. The Hilbert transform can be defined in the frequency domain as $f_{Hi}(x) \circ\!\!-\!\!\bullet\, F_{Hi}(u) = -iu/|u|F(u)$, where F denotes the Fourier transform of f. We set $F_{Hi}(0) = 0$. The analytic signal $f_A = f + if_{Hi}$ is then given as

$$f_A(x) = a(x)\exp(i2\pi u(x)x), \tag{4}$$

such that the local phase can be retrieved as $\phi(x) = \arg(f_A(x)) = 2\pi u(x)x$. See Hahn [9] for more details on the Hilbert transform and the analytic signal.

This concept is usually applied to discrete finite signals f_n in combination with a bandpass filter. One such construction is the *lognormal filter* introduced by Knutsson [12]. The transfer function of the lognormal filter is

$$R(u) = \begin{cases} e^{-\frac{4}{B^2\ln(2)}\ln^2(u/u_c)} & \text{if } u > 0 \\ 0 & \text{else} \end{cases}. \tag{5}$$

Here the relative bandwidth B is given by.

$$B = \frac{1}{\ln(2)}\ln\left(\frac{u_u}{u_l}\right). \tag{6}$$

[1]This can be achieved – up to the restrictions made in the introduction – if $a(x)$ and $\cos(2\pi u(x)x)$ have disjunct support in the frequency domain, where all frequencies contained in $a(x)$ are lower than all frequencies of $\cos(2\pi u(x)x)$. See [2] for details. We assume that this condition is fulfilled in the following.

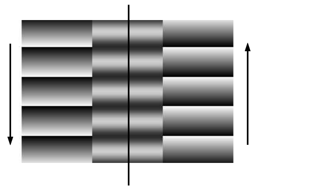

Figure 2: The image in the center has constant local orientation (horizontal). The local phase is thus evaluated normal to that orientation (vertical). Depending on which direction is chosen, the two different phase images to the left and the right of the signal can be found.

The maximum of R is found to be $R(u_c)$. The frequencies u_l and u_u are the lower and the upper frequency, respectively, where R falls to half its maximum: $R(u_u) = R(u_l) = 0.5R(u_c)$. The application of the lognormal filter leads to an analytic signal, since it suppresses all negative frequencies. At the same time it cancels the DC-component and high frequency noise, while admitting a wide passband. We will use this filter and its 2D extension in the following section.

2.2. Phase in 2D

The concept of local phase of a signal introduced above can be extended to 2D signals (images) if those signals are *simple*. An image is called simple, if it is locally constant with respect to one orientation and its variation can be described with respect to the normal orientation. These orientations may vary within the image. The Moiré interferograms which are addressed in this article are simple signals.

The orientation of the constant component is called the *local orientation* of the signal. The local phase can be defined to be the 1D local phase normal to the local orientation. However the problem occurs that the orientation along which the phase is to be evaluated is defined, but not the direction. In 1D the phase was defined to be a monotonically increasing function (up to wrap-arounds). This is no longer possible in 2D. Figure 2 clarifies the situation.

In order to remove this ambiguity from the definition of the local phase in 2D Granlund [7] proposes to store the local phase together with the direction of evaluation in a unique three-vector Φ:

$$\mathbf{\Phi}(x,y) = \begin{pmatrix} \cos(\alpha(x,y))\sin(\phi(x,y)) \\ \sin(\alpha(x,y))\sin(\phi(x,y)) \\ \cos(\phi(x,y)) \end{pmatrix} \tag{7}$$

Here, $\alpha(x,y)$ is the direction along which the local phase $\phi(x,y)$ is evaluated. This direction is normal to the local orientation of the image. In the following we will work with the *normal direction* α.

From the above analysis it follows that neither the local phase ϕ nor the normal direction α can be uniquely extracted from the image: The normal direction α can be replaced by $\alpha \pm \pi$ which would force ϕ to be replaced by $-\phi$. The power of (7) is that $\mathbf{\Phi}$ is invariant to this change and therefore is unique:

$$\begin{pmatrix} \cos(\alpha)\sin(\phi) \\ \sin(\alpha)\sin(\phi) \\ \cos(\phi) \end{pmatrix} = \begin{pmatrix} \cos(\alpha \pm \pi)\sin(-\phi) \\ \sin(\alpha \pm \pi)\sin(-\phi) \\ \cos(-\phi) \end{pmatrix}. \tag{8}$$

In Sect. 3 we will describe two ways to estimate $\mathbf{\Phi}$ from images. Before that, we show how $\mathbf{\Phi}$ can be used in order to solve the "phase-flipping" problem stated in the introduction.

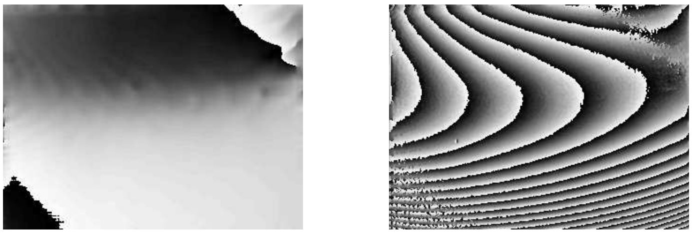

(a) **(b)**

Figure 3: One possible solution of the normal direction/phase splitting of the phase vector Φ applied to Fig. 1(b). **(a)** The normal direction α according to (9). **(b)** The local phase according to 10. Inconsistencies can be seen in the lower left and in the upper right corner. These inconsistencies make the surface reconstruction impossible in these regions.

2.3. Direction Unwrapping

Having obtained the phase vector $\mathbf{\Phi}$ (we will show how that can be done in Sect. 3) we can split it into a first guess of α and ϕ. One way to do this is

$$\alpha = \text{atan}(\Phi_2/\Phi_1) \tag{9}$$

$$\phi = \text{atan2}(\text{sign}(\Phi_1)(\Phi_1^2+\Phi_2^2), \Phi_3) \tag{10}$$

Here, atan2 denotes the sign-dependent arcus-tangens function. Thus, α is defined within the interval $(-\pi/2, \pi/2]$, while ϕ is defined within $(-\pi, \pi]$. This separation for the Moiré interferogram in Fig. 1(b) is shown in Fig. 3.

It can be seen from Fig. 3 that the normal direction wraps around by $\pm\pi$ in the lower left and the upper right corner of the image. Consequently the phase ϕ flips its sign in these areas. We can use our freedom of changing α and ϕ simultaneously while keeping $\mathbf{\Phi}$ constant. The direction wrap-arounds are easily detectable, because all over the image the orientation changes smoothly (this holds for all interferograms under consideration). Positions with differences in α between neighboring pixels of more than $\pi/2$ can be identified as wrap-arounds.

A simple method for 1D phase-unwrapping is the method of Itoh [10]. This method first calculates discrete phase differences between neighboring pixels. The unwrapped phase is than evaluated by starting from the leftmost phase-value and integrating up the wrapped phase differences.

This method can directly be applied to direction unwrapping. We apply Itoh's method to the normal direction image α line-wise. To the result the same method is applied columnwise. Thanks to the rather simple structure of the interferograms this method has been successful in all our experiments.

During the direction unwrapping process some pixels are shifted by $\pi + k2\pi,\ k \in \mathbb{Z}$ and some by $k2\pi,\ k \in \mathbb{Z}$. For the solution of the "phase-flip" problem we merely have to invert the phase-values from ϕ to $-\phi$ at position where the direction has been changed by an odd multiple of π. Thus, $\mathbf{\Phi}$ stays unchanged. This is the core of our method: We shift the problem of a consistent phase-estimation from the phase domain to the direction domain, where it can be solved with extremely simple methods. In the phase-domain itself the problem is much harder to solve.

The result of direction unwrapping and the corresponding correction of the phase-image is shown in Fig. 4. The results for the model wing from Fig. 1(a) are shown in Fig. 5.

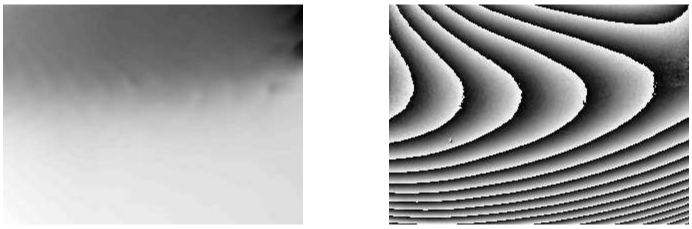

(a) (b)

Figure 4: The final results. **(a)** The direction image Fig. 3(a) after direction unwrapping. **(b)** The phase image Fig. 3(b) after the inversion of the phase-values as indicated by the unwrapped direction values.

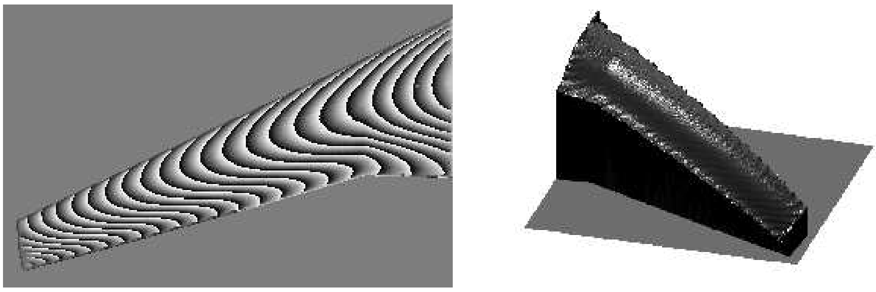

(a) (b)

Figure 5: The final result for the model wing. **(a)** The phase image Fig. 3(b) after the inversion of the phase-values as indicated by the unwrapped direction values. **(b)** The unwrapped phase-image as surface plot. This corresponds directly to the surface shape of the real model.

In the following section we present two methods for the estimation of $\mathbf{\Phi}$ and compare their accuracy in their estimation of ϕ.

3. Estimation of 2D Phase

3.1. Lognormal Filter

Knutsson [11] proposed to use a set of $N \geq 3$ polar separable filters. The transfer functions of his filters are given by

$$H_k(\boldsymbol{u}) = R(|\boldsymbol{u}|)D_k(\boldsymbol{n}), \tag{11}$$

where $\boldsymbol{u} = (u, v)$ denotes the 2D frequency coordinates. R is the radial component of the filter, while D is the directional component which only depends on $\boldsymbol{n} = \boldsymbol{u}/|\boldsymbol{u}|$.

The radial component is identical for all filters H_k. It is chosen to be the lognormal filter as defined in (5). The directional component D_k is given by

$$D_k(\boldsymbol{n}) = \begin{cases} [\boldsymbol{n} \cdot \boldsymbol{n}_k]^2 & \text{if } \boldsymbol{n} \cdot \boldsymbol{n}_k > 0 \\ 0 & \text{else.} \end{cases} \tag{12}$$

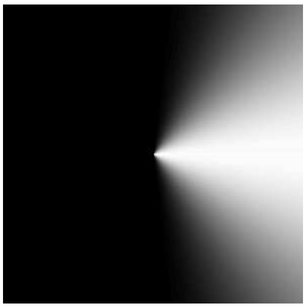

Figure 6: The transfer function of a directional lognormal filter

with $\boldsymbol{n}_k = (\cos(\alpha_k), \sin(\alpha_k))^T$ and $\alpha_k = k\pi/(N+1)$. Figure 6 shows the transfer function of a typical filter H_k. These filters evaluate an analytic signal with respect to the direction $\boldsymbol{n}_k$ since they suppress all frequency component in the frequency-halfplane $\boldsymbol{u} \cdot \boldsymbol{n}_k \leq 0$.

From the filter responses

$$f_k(\boldsymbol{x}) \circ\!\!-\!\!\bullet\ F_k(\boldsymbol{u}) = F(\boldsymbol{u})H_k(\boldsymbol{u}) \tag{13}$$

to an image f we recover the local normal direction $\alpha(\boldsymbol{x})$ and the local phase $\phi(\boldsymbol{x})$ as follows: $\alpha(\boldsymbol{x}) = \alpha_k$, where k is such that

$$|f_k(\boldsymbol{x})| = \max_{l\in\{1\ldots N\}}\{|f_l(\boldsymbol{x})|\}. \tag{14}$$

Analogously $\phi(\boldsymbol{x})$ is defined as $\phi(\boldsymbol{x}) = \arg(f_k(\boldsymbol{x}))$ where k is again evaluated from (14). The functions α and ϕ form a basis from which we can derive the consistent phase-image by applying direction unwrapping. Results on the accuracy of ϕ will be presented in Sect. 4.

3.2. Riesz-Filter

This approach is based on a 2D extension of the analytic signal presented in [5]. This method is based on Riesz transforms. In contrast to the lognormal filter presented above, the vector $\boldsymbol{\Phi}$ is estimated directly here.

In the introduction it was shown how the phase of a 1D signal can be estimated by the construction of the analytic signal which is a combination of the original signal and its Hilbert transform. The transfer function of the 1D Hilbert transform is given by $H(u) = -iu/|u|$. A surprisingly straightforward extension yields the transfer function $\boldsymbol{R}(\boldsymbol{u})$ of the 2D Riesz transform:

$$\boldsymbol{R}(\boldsymbol{u}) = -i\boldsymbol{u}/|\boldsymbol{u}|, \text{ with } \boldsymbol{u} = (u,v)^T \neq (0,0)^T. \tag{15}$$

We define $\boldsymbol{R}(\mathbf{0}) = \mathbf{0}$. Riesz transforms are well-known to mathematicians as nD extensions of the Hilbert transform [17]. They have been applied to the analysis of geophysical data in [14, 15].

The Riesz transform of a 2-D signal f is given by

$$\begin{pmatrix} f_{r1}(\boldsymbol{x}) \\ f_{r2}(\boldsymbol{x}) \end{pmatrix} \circ\!\!-\!\!\bullet\ -i\begin{pmatrix} \cos(\alpha) \\ \sin(\alpha) \end{pmatrix} F(\boldsymbol{u}), \tag{16}$$

where the Fourier transform is performed component wise and α is the angle between $\boldsymbol{u} = (u,v)^T$ and the u-axis.

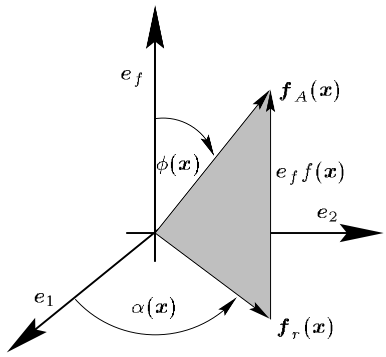

Figure 7: The combination of the input signal f and its Riesz transform $\boldsymbol{f}_r$ into the vector-valued function $\boldsymbol{f}_A$.

As in 1D the analytic signal is a combination of the Hilbert transform and the original signal, a 2D version of the analytic signal can be defined as the combination of the Riesz transforms of the image and the image itself:

$$\boldsymbol{f}_A = f\boldsymbol{e}_f + f_{r1}\boldsymbol{e}_1 + f_{r2}\boldsymbol{e}_2, \tag{17}$$

where $\{\boldsymbol{e}_f, \boldsymbol{e}_1, \boldsymbol{e}_2\}$ is an orthonormal basis of $\mathbb{R}^3$. This vector is visualized in Fig. 7. It turns out that the norm of $\boldsymbol{f}_A$ is an estimate for the phase vector $\boldsymbol{\Phi}$:

$$\boldsymbol{\Phi}_{est}(\boldsymbol{x}) = |\boldsymbol{f}_A(\boldsymbol{x})|. \tag{18}$$

Thus, starting from this estimate we can apply the direction unwrapping approach as described above in order to derive a consistent phase image.

4. Experiments

4.1. The Data

Since we have no ground truth for the real Moiré interferograms shown in Fig. 1 we produce synthetic interferograms in order to compare the quality of the ϕ estimates of the two approaches presented above.

In order to generate synthetic Moiré interferograms we first produce depth data of the form

$$z(\boldsymbol{x}) = a_1x^2 + a_2y^2 + a_3x + a_4y + a_5xy + a_6\sin(x), \tag{19}$$

where the a_i are randomly chosen from the interval $[0, 20]$. The depth data is then wrapped by

$$\phi(\boldsymbol{x}) = \text{atan2}(\sin(z(\boldsymbol{x})), \cos(z(\boldsymbol{x}))). \tag{20}$$

Finally the interferogram is generated by

$$f(\boldsymbol{x}) = \cos(\phi) + noise, \tag{21}$$

where uniform noise from the interval $[-0.2, 0.2]$ is added. A typical synthetic interferogram is shown in Fig. 8. We exclude interferograms which contain local extrema of z within the field of view, which is consistent with the real data. The real experimental setup is especially designed in order to avoid these extrema, since they cause low frequency of the Moiré pattern, which results in poorer phase-estimates.

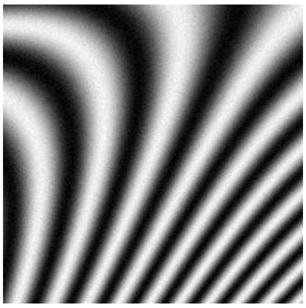

Figure 8: A synthetically generated Moiré interferogram.

4.2. Regularization of the Riesz-Orientation Map

A problem that we encounter in the Riesz approach are singularities of the orientation at positions of $\phi = 0, \pm\pi$. It can be seen from Fig. 7 that the vector $\boldsymbol{f}_A$ is normal to the $\boldsymbol{e}_1, \boldsymbol{e}_2$-plane, which makes it impossible to retrieve α.

In [4] this problem is solved by averaging α within a small region. Since $|\sin(\phi)|$ can serve as a confidence measure for the correctness of the α estimate we use *normalized convolution* as introduced by Knutsson et al. [13] in order to weigh the value corresponding to their reliability in the averaging:

$$\alpha_{av}(m,n) = \arg(\sum_{(m,n)\in\mathcal{N}(m,n)} (W_\alpha(m,n)) * box_M))/2 \tag{22}$$

where

$$W_\alpha(m,n) = \exp(i2\alpha(m,n) conf_\alpha(m,n) \tag{23}$$

and $conf_\alpha$ is the confidence measure for α which will be analyzed in more detail: Felsberg [4] uses the confidence measure

$$conf_\alpha^2 = \sin^2(\phi). \tag{24}$$

We will show that the confidence measure (24) punishes positions with intermediate values of $|\sin(\phi)|$ stronger than necessary in the current application. We propose to use a confidence map of the form

$$conf_\alpha^k = |\sin(\phi)|^k \tag{25}$$

where we estimate an appropriate value of k from synthetic Moiré interferograms with known orientation ground-truth in the following way: Let $\alpha(m,n)$ and $\alpha_{est}(m,n)$ the true and the estimated orientation field, respectively. The estimated image-phase is denoted by $\phi_{est}(m,n)$. We define the accuracy of α_{est} as

$$acc_\alpha(m,n) := 1 - \frac{err_\alpha(m,n)}{\pi/2}, \tag{26}$$

where the error of the orientation estimate err_α is given by

$$err_\alpha(m,n) := \arg(\exp(i2(\alpha(m,n) - \alpha_{est}(m,n))))/2. \tag{27}$$

We chose $k \in \mathbb{R}$ such that

$$\sum_{m,n} |acc_\alpha(m,n) - |\sin(\phi_{est}(m,n))|^k| \to min. \tag{28}$$

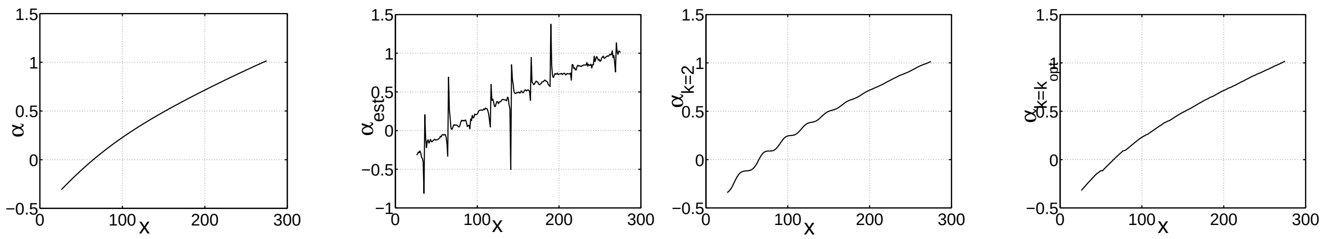

(a) **(b)** **(c)** **(d)**

Figure 9: Regularization of the orientation estimate obtained from the Riesz-transforms. **(a)** One row of the true orientation α of a synthetically generated Moiré interferogram. **(b)** The estimated orientation α_{est} before regularization. **(c)** α_{est} after regularization using the confidence map (25) with $k = 2$. **(d)** Orientation after regularization using $k = 0.1183$.

Using a set of 100 synthetically generated interferograms we find an average value of $k_{opt} = 0.1183$ with a standard deviation of $\sigma(k) = 0.0004$. Figure 9 shows the different effects of using $k = 2$ and $k = k_{opt}$. It can be seen that the usage of $k = 2$ leads to a the introduction of steps in the orientation image. This is a consequence of underestimating the reliablility of orientation values which lie close to singularities. The average absolute error of the estimated orientation in another test-set of 100 synthetically generated interferograms was $\overline{(err_\alpha)_{k=2}} = 1.33\%$ and $\overline{(err_\alpha)_{k=k_{opt}}} = 0.89\%$. Thus, the average orientation error could be reduced by more than 30% by the use of k_{opt}.

4.3. Results

In experiments we apply the same parameters for the radial lognormal filter. These are $u_l = 0.1$, $u_c = 0.4$ and $u_u = 2$, where u ranges on a scale from $-\pi$ to π. This bandpass filter is also applied to the interferograms before the Riesz-transform is used.

In all our experiments the direction unwrapping method described earlier is successful. In this respect both approaches, Knutsson's lognormal filter with $3 \leq N \leq 8$ or the Riesz transform approach are equally good.

Using a test set of 20 synthetic Moiré interferograms we find a mean absolute error for ϕ of about 1.4% for the lognormal filter approach. This error is interestingly not observably dependent of N, when chosen from $\{3, 4, 5, 6, 7, 8\}$. The mean absolute error in the experiments using the Riesz transform approach was about 1.3%.

5. Conclusions and Future Work

We have presented a method for the consistent estimation of local phase from Moiré interferograms. The key feature of our approach is the simultaneous use of local phase and local orientation information. We could show that the task of phase correction is equivalent to unwrapping the direction image. The latter is a much simpler task. In all our experiments a very simple unwrapping algorithm was successful.

We investigated two methods for the estimation of the phase vector Φ. From our experiments it seems the the Riesz transform approach is preferable over the lognormal filter approach: The first yields a more correct phase estimate. Since the difference is rather small, this should be investigated in more detail, however. Furthermore the Riesz approach is of lower complexity, since only two transforms have to be calculated in comparison to at least three for Knutsson's lognormal filters. The extra step of orientation regularization which is required in the Riesz transform approach is less expensive than an extra transform.

There exist more sophisticated phase unwrapping algorithms than the one used in this paper for direction unwrapping (see e.g. [8]). Although the simple unwrapping approach based on Itoh's method was successful in all experiments, future work should aim at the adaptation of these approaches to direction unwrapping, since more noise in the data or a local extremum of z within the field of view could cause our approach to fail. Furthermore an automatic method should be developed which indicates whether the direction unwrapping was successful or not.

Acknowledgments

The work reported here was initiated while the author was a postdoctoral researcher at the Cognitive Systems group at the University of Kiel, Germany, working with G. Sommer whose interest and support is gratefully acknowledged. The work was supported by the *Deutsche Forschungsgemeinschaft (DFG)* (Grant: Bu 1259/2). The author would also like to thank D. Pallek (DLR, Göttingen, Germany) for helpful discussions and for providing the interferograms (Fig. 1) used in our experiments.

References

[1] P.H. Baumann and K.A. Bütefisch. Measurement of hinge moments and model deformations in wind tunnels by means of Moiré interferometry. In S.S. Cha and J.D. Trolinger, editors, *Optical Techniques in Fluid, Therma, and Combustion Flow*, volume 2546, pages 16–32. SPIE, July 1995.

[2] B. Boashash. Estimating and interpreting the instantaneous frequency of a signals—part 1: Fundamentals. *Proceedings of the IEEE*, 80(4):520–538, 1992.

[3] Th. Bülow, D. Pallek, and G. Sommer. Riesz transforms for the isotropic estimation of the local phase of Moiré interferograms. In G. Sommer, editor, *Mustererkennung 2000, 22. DAGM-Symposium*, pages 333 – 340, Kiel, 2000.

[4] M. Felsberg and G. Sommer. A new extension of linear signal processing for estimating local properties and detecting features. In G. Sommer, editor, *Mustererkennung 2000, 22. DAGM-Symposium*, pages 195–202, Kiel, 2000.

[5] M. Felsberg and G. Sommer. Structure multivector for local analysis of images. Technical Report 2001, Institute of Computer Science and Applied Mathematics, Christian-Albrechts-University of Kiel, Germany, February 2000.

[6] D. Gabor. Theory of communication. *Journal of the IEE*, 93:429–457, 1946.

[7] G.H.Granlund and H. Knutsson. *Signal Processing for Computer Vision*. Kluwer Academic Publishers, 1995.

[8] C.G. Ghiglia and M.D. Pritt. *Two-Dimensional Phase Unwrapping, Theory, Algorithms, and Software*. John Wiley & Sons, Inc., 1998.

[9] S. L. Hahn. *Hilbert Transforms in Signal Processing*. Artech House, Boston, London, 1996.

[10] K. Itoh. Analysis of the phase unwrapping problem. *Applied Optics*, 21(14):2470, 1982.

[11] H. Knutsson. *Filtering and Reconstruction in Image Processing*. PhD thesis, Linköping University, Sweden, 1982.

[12] H. Knutsson, B. von Post, and G.H. Granlund. Optimization of arithmetic neighborhood operations for image processing. In *1st Scandinavian Conference on Image Analysis*, 1980.

[13] H. Knutsson and C.F. Westin. Normalized and differential convolution: Methods for interpolation and filtering of incomplete and uncertain data. In *CVPR*, 1993.

[14] Misac N. Nabighian. The analytic signal of two-dimensional magnetic bodies with polygonal cross-section: its properties and use for automated anomaly interpretation. *Geophysics*, 37(3):507–517, June 1972.

[15] Misac N. Nabighian. Toward a three-dimensional automatic interpretation of potential field data via generalized Hilbert transforms: Fundamental relations. *Geophysics*, 49(6):780–786, June 1984.

[16] D. Pallek, P.H. Baumann, K.A. Bütefisch, and J. Kompenhans. Application of Moiré interferometry for model deformation measurements in large scale wind tunnels. In T.A. Kowalewski, W. Kosinski, and J. Kompenhans, editors, *Euromech 406 Colloquium, Image Processing Methods in Applied Mechanics*, pages 167–170, Warsaw, 1999.

[17] E.M. Stein and G. Weiss. *Introduction to Fourier Analysis on Euclidean Spaces*. Princeton University Press, New Jersey, 1971.